Alinejad, Farid; Bordbar, Hadi; Hostikka, Simo

# Improving the modeling of spectral radiation penetration into the condensed materials with the separated full spectrum correlated-k method

*Published in:*
International Journal of Heat and Mass Transfer

*DOI:*
10.1016/j.ijheatmasstransfer.2021.121448

Published: 01/09/2021

*Document Version*
Publisher's PDF, also known as Version of record

International Journal of Heat and Mass Transfer 176 (2021) 121448

Contents lists available at ScienceDirect

International Journal of Heat and Mass Transfer

journal homepage: www.elsevier.com/locate/hmt

# Improving the modeling of spectral radiation penetration into the condensed materials with the separated full spectrum correlated-k method

Farid Alinejad, Hadi Bordbar*, Simo Hostikka

*Department of Civil Engineering, School of Engineering, Aalto University, Finland*

ARTICLE INFO

*Article history:*
Received 19 March 2021
Revised 26 April 2021
Accepted 4 May 2021
Available online 5 June 2021

*Keywords:*
Spectral radiation transfer
Condensed materials
Separated FSCK method
Compact FSCK method
Reference temperature
Medium emission

ABSTRACT

The large temperature difference between the radiation source and the condensed materials in fire scenarios, makes the general form of full spectrum correlated-k method unable to accurately model both absorption and emission within the condensed phase. In this paper, a new solution form for the FSCK method is presented which accurately accounts for both. This so-called "separated" form of FSCK method solves the contributions of medium emission and boundary's incident intensity separately by implementing two different reference temperatures. The advantages of the separated FSCK method is exhibited through three case studies using the transmissivity and radiative heat source calculated by high resolution line by line calculations as the benchmark. The test cases represent a layer of six different liquid and solid hydrocarbon fuels for which the various levels of irradiation from a radiating source is introduced by the temperature of its upper wall and an effective emissivity. The case studies provide a sensitivity analysis for the magnitude and spectral form of the irradiation at the boundary. The separated form of FSCK exhibits its best performance when the incident intensity and medium emission are in the same order of magnitude. Moreover, when the peak region of the boundary's spectral irradiation is closer to the peaks of the absorption coefficient spectrum of the condensed phase, the accuracy of both separated and classical FSCK solutions decreases, though, the separated solution still provides better accuracy.



## 1. Introduction

The recent progress in computational resources paved the road for high fidelity numerical modeling of complex physical phenomena occuring in energy conversion processes such as multiphase flows [1,2] and thermal radiation [3,4]. Spectral radiative heat transfer in gaseous combustion products has been extensively studied in past years and several methods such as weighted sum of gray gases (WSGG) [5–7], spectral line based weighted sum of gray gases (SLW) [8,9], and full spectrum correlated k-distribution (FSCK) [10,11] methods have been presented for its modeling. In contrary, radiation transfer modeling within the condensed materials has been simplified to gray modeling using an average value for the absorption coefficient of the material and solving the radiative transfer equation (RTE) only once. It has been conventionally justified by the smoother profile of the spectral absorption coefficient, lower temperatures, and strong absorption of the condensed materials compared to gaseous combustion products. However, recent studies showed that radiation transfer in liquids is more complex and applying the gray assumption may result in inaccurate estimation of the radiative heat source and heat flux [12,13] especially in the first layers of the materials which may undergo a phase transition in combustion scenarios.

The first attempt to include more detailed spectral absorption in modeling radiative heat transfer in the liquid fuels was done by Isojärvi et al. [12] implementing the k-distribution method to estimate the transmissivity of the incident intensity within liquid heptane ignoring the effect of medium emission. They extracted the k-distribution of liquid heptane by using the flame irradiation spectrum at the liquid surface of a 2m pool fire experimentally measured by Suo-Antilla et al. [14]. To account for liquid emission, Alinejad et al. [13] developed the full spectrum correlated-k distribution method for liquid fuels by presenting look-up tables for five liquid fuels including decane, ethanol, ethylene glycol, heptane, and toluene. They showed that applying the flame temperature or equivalent Planck temperature of the incident intensity at the surface of the liquid as the reference temperature in FSCK method gives the most accurate results. However, their simulations

* Corresponding author.
*E-mail address:* hadi.bordbar@aalto.fi (H. Bordbar).

https://doi.org/10.1016/j.ijheatmasstransfer.2021.121448

**Latin**

| | |
|---|---|
| $a$ | The ratio of any two full spectrum k-distributions |
| $f$ | K-distribution function |
| $g$ | Cumulative k-distribution function |
| $I$ | Total intensity ($W/m^2/sr$) |
| $I_b$ | Blackbody total intensity ($W/m^2/sr$) |
| $I_{b\lambda}$ | Blackbody spectral intensity ($W/m^2/\mu m/sr$) |
| $I_g^+$ | Forward intensity in $g$ space ($W/m^2/sr$) |
| $I_g^-$ | Backward intensity in $g$ space ($W/m^2/sr$) |
| $I_m^+$ | Forward total intensity due to the liquid emission ($W/m^2/sr$) |
| $I_{mg}^+$ | Forward intensity due to the liquid emission in $g$ space ($W/m^2/sr$) |
| $I_{mg}^-$ | Backward intensity due to the liquid emission in $g$ space ($W/m^2/sr$) |
| $I_{m\lambda}^+$ | Forward spectral intensity due to the liquid emission ($W/m^2/\mu m/sr$) |
| $I_{m\lambda}^-$ | Backward spectral intensity due to the liquid emission ($W/m^2/\mu m/sr$) |
| $I_w^+$ | Forward total intensity due to the incident intensity ($W/m^2/sr$) |
| $I_{wg}^+$ | Forward intensity due to the incident intensity in $g$ space ($W/m^2/sr$) |
| $I_{wg}^-$ | Backward intensity due to the incident intensity in $g$ space ($W/m^2/sr$) |
| $I_{w\lambda}^+$ | Forward spectral intensity due to the incident intensity ($W/m^2/\mu m/sr$) |
| $I_{w\lambda}^-$ | Backward spectral intensity due to the incident intensity ($W/m^2/\mu m/sr$) |
| $I_\lambda^+$ | Forward spectral intensity ($W/m^2/\mu m/sr$) |
| $I_\lambda^-$ | Backward spectral intensity ($W/m^2/\mu m/sr$) |
| $k$ | Correlated k-value ($m^{-1}$) |
| $L$ | Thickness of the fuel layer (m) |
| $\hat{n}$ | Unit normal vector |
| $(\dot{q}'')^+$ | Forward heat flux ($W/m^2$) |
| $(\dot{q}'')^-$ | Backward heat flux ($W/m^2$) |
| $\dot{q}'''_{rad}$ | Heat source ($W/m^3$) |
| $\hat{s}$ | Unit direction vector |
| $T$ | Temperature ($K$) |
| $w$ | Weighting parameter |
| $x$ | Path length (m) |

*Greek*

| | |
|---|---|
| $\varepsilon$ | Emissivity |
| $\kappa_\lambda$ | Absorption coefficient ($1/m$) |
| $\lambda$ | Wavelength ($\mu m$) |
| $\tau$ | Transmissivity |
| $\Omega$ | Solid angle ($sr$) |

*Subscript*

| | |
|---|---|
| $avg$ | Average |
| $bw$ | Bottom wall |
| $in$ | Input |
| $out$ | Output |
| $ref$ | Reference |
| $uw$ | Upper wall |

*Abbreviation*

| | |
|---|---|
| FSCK | Full spectrum correlated-k distribution |
| HR | High resolution |
| PMMA | Poly (methyl methacrylate) |
| QP | Quadrature point |
| RC-FSK | Rank correlated full spectrum k-distribution |
| RTE | Radiative transfer equation |
| SLW | Spectral line-based weighted sum of gray gases |
| WSGG | Weighted sum of gray gases |

were carried out for the direct flame condition with applying of an equivalent flame temperature of 1450 K reported in [14]. The FSCK method is sensitive to the selection of reference temperature. To eliminate this problem, Solovjov et al. [15] presented the rank correlated-FSK (RC-FSK) method that does not need selecting a reference state in applying the FSCK method. In condensed materials, we usually do not deal with the changes of concentration of materials and the thermodynamic state can be explained by a temperature only. Moreover, the changes of absorption spectra with the medium temperature is also negligible [16,17]. Hence, for a considered reference temperature, a fixed set of k values can be applied. Therefore, the RC-FSK method, which brought great advantages to spectral radiation modeling in gas phase, is expected to not show its privileges in solving spectral radiation penetration in condensed materials.

In both of these recent works [12,13], the simulations have been done for the flame condition reported for the large pool fire in [14]. Applying the flame irradiation to the pool for generating k-distribution, the incident intensity showed the largest contribution to the radiative intensity inside the liquid and encourages neglecting the medium emission due to the medium low temperature. The source of incident radiation at the boundary of the condensed materials can be hot gases or other flames rather than the combustion flame of the condensed phase itself. Considering the flame emissivity, view factor, and reflection from the material surface, the boundary incident radiation, and medium emission can be in a same order of magnitude. Therefore, in such a scenario, the role of medium emission can be significant and should not be ignored. The amount of the medium emission depends on the temperature and absorption coefficient of the material. Hence, solids and liquids with high boiling temperature and high absorption coefficient such as heavy hydrocarbons may strongly emit radiation. It was shown that by using the flame temperature as the reference temperature in FSCK calculations of liquid heptane and toluene, the liquid emission is not accurately solved [18]. It triggered the motivation of the current work to improve the accuracy of FSCK method in the simulation of both absorption and emission within the condensed materials.

The new formulation of FSCK presented in the current work is based on separating the contributions of medium emission and irradiation at boundary of a condensed material layer. The history of this idea goes back to the work by Olef [19] in introducing a modified differential approximation for solving the RTE within gaseous media. In this method, radiative transfer equation (RTE) is written based on radiative heat flux instead of radiation intensity. While the radiative heat flux due to medium emission is isotropic, the radiative heat flux due to irradiation at boundaries is not. Hence, the ordinary differential approximation can not accurately solve the thermal radiation within a layer of condensed materials. To tackle this issue, radiative heat flux was assumed to consist of two parts: 1) the heat flux due to the walls' emission and 2) the heat flux due to the gas emission. Solving the former one analytically and the latter one numerically, Olef presented the modified differential approximation method for nonscattering media. Neglecting the in-scattering term of the wall emission, Modest [20] generalized this approach by applying it to a three-dimensional scattering medium. Implementing the same approach, Ramankutty and Crosbie [21,22] developed the modified discrete ordinates method which is still a popular method in the radiation transfer simulations used by different researchers [23,24].

Taking advantage of the basic idea of the separation technique, we improve the accuracy of FSCK method in solving the radiation heat transfer within the condensed materials in combustion environments. We derive two different RTEs for the FSCK method to accurately calculate contributions of flame irradiation at the boundary and emission of the condensed materials. Accordingly, in the next section, the separated form of FSCK is developed to solve radiation heat transfer into a layer of the condensed materials. In Section 3, the new model will be validated through several test cases paving the road to address the sensitivity of the model in various thermal conditions of the considered system. Results of the novel separated FSCK method compared to those of the original FSCK method will come in Section 4. Finally, Section 5 summarizes the most important contributions and results of the present research.

## 2. Theory

### 2.1. The original (compact) FSCK method

To estimate radiation heat transfer in participating media, the radiative transfer equation (RTE) is solved for radiation intensity at different locations and directions. Neglecting scattering, the two flux form of the RTE can be written as:

$$\frac{1}{2}\frac{dI_\lambda^+}{dx} = \kappa_\lambda I_{b\lambda} - \kappa_\lambda I_\lambda^+ \tag{1}$$

where, $I_\lambda^+$, $I_{b\lambda}$ $\kappa_\lambda$, and $x$ are forward spectral intensity, blackbody spectral intensity, absorption coefficient, and path length, respectively. For the sake of simplicity, the two-flux method [25] has been used for modeling directional dependency of the radiation heat transfer in the present work. Nonetheless, the present approach is readily applicable to the general form of RTE for non-scattering media.

The boundary condition for Eq. (1) is written as:

$$I_\lambda^+(0) = \varepsilon_{uw}\varepsilon_{flame} I_{b\lambda}(T_{uw}) + \frac{1-\varepsilon_{uw}}{\pi}\int_{\hat{n}.\hat{s}<0} I_\lambda^-(0)|\hat{n}.\hat{s}|d\Omega \tag{2}$$

where $\varepsilon_{uw}$, $\varepsilon_{flame}$, $T_{uw}$, $I_\lambda^-$, $\Omega$, $\hat{n}$, and $\hat{s}$ are diffuse emissivity of the upper wall, emissivity of the flame, the temperature of the upper wall, backward spectral intensity, solid angle, unit normal vector, and direction vector, respectively. The irradiation reaching the upper wall of the condensed material from a source of radiation, for instance a flame, is represented by a Planck intensity profile of a blackbody at a temperature, e.g. the flame temperature, times a flame emissivity. The flame emissivity ($\varepsilon_{flame}$) represents the self-absorption of flame radiation caused by hot combustion products or for instance by the cold fuel rich region above the condensed materials. The upper wall's emissivity ($\varepsilon_{uw}$) used in Eq. (2) accounts for the reflection of the upper surface of the condensed materials. Considering the spectral variation of absorption coefficient of the condensed materials, the RTE should be solved for fine enough spectral intervals to provide the benchmark solutions of the test cases. In this paper, this solution is called "high-resolution (HR)" which has an analogy to the LBL solutions used in gas spectral radiation research. To solve Eq. (1), the reported spectral absorption coefficients and the spectrally averaged refractive indexes in [13] are used for five liquid fuels including decane, ethanol, ethylene glycol, heptane, and toluene. For clear poly methyl methacrylate(PMMA), the reported spectral absorption coefficients in [26] and the averaged value of 1.48 for the refractive index are applied. While the HR solution is computationally demanding, the FSCK method provides a fast and accurate way to account for spectral thermal radiation. Applying two flux method for directional dependency, the RTE for the FSCK method is generally given as [13]:

$$\frac{1}{2}\frac{dI_g^+}{dx} = k(a(T, T_{ref}, g_{ref})I_b(T) - I_g^+) \tag{3}$$

where $I_g^+$, $I_b$, $a$, and $k$ are the intensity in the g space, total blackbody intensity, the ratio of two full spectrum k-distributions of local to reference states, and the correlated absorption coefficient, respectively. A more detailed description of these parameters can be found in [13] and [27]. They will also be briefly introduced in the next subsection where the new separated form of the FSCK method is presented. The boundary condition for the FSCK method is given as:

$$I_g^+(0) = \varepsilon_{uw}\varepsilon_{flame} I_b(T_{uw}) + \frac{1-\varepsilon_{uw}}{\pi}\int_{\hat{n}.\hat{s}<0} I_g^-(0)|\hat{n}.\hat{s}|d\Omega \tag{4}$$

where $I_g^-$ is the backward intensity in the $g$ space. In this paper, we call the original form of FSCK presented by Eqs. (3) and (4) the compact form of the FSCK method. The RTE and boundary condition for the backward radiation are written in a similar way [13]. To apply the compact form of the FSCK method, only one reference temperature needs to be chosen for the whole domain. It is shown that using an equivalent flame temperature as the reference temperature in the FSCK calculations results in the highest accuracy compared to other suggested reference temperatures in the literature such as volume averaged and Planck-mean temperatures [13].

### 2.2. The separated FSCK method

Due to the large difference between the flame temperature and the medium temperature in fire scenarios of condensed materials, the original FSCK using a single reference temperature may not be able to accurately solve the spectral radiation within the condensed material, especially where the flame irradiation is not dominant and the liquid emission is of relative importance [18]. This is caused by applying the source temperature as the reference temperature for both absorption of boundary's irradiation and medium emission.

To solve this issue, the radiation intensity within the medium for forward direction can be written as the sum of the contributions of the intensity originated from incident radiation at boundary ($I_{w\lambda}^+$) and the intensity originated from medium emission ($I_{m\lambda}^+$) as:

$$I_\lambda^+(\hat{s}) = I_{m\lambda}^+(\hat{s}) + I_{w\lambda}^+(\hat{s}) \tag{5}$$

Substituting the above equation into Eq. (1) and separating the RTE for the two introduced new intensities, the following equation for $I_{m\lambda}^+$ is obtained:

$$\frac{1}{2}\frac{dI_{m\lambda}^+}{dx} = \kappa_\lambda I_{b\lambda} - \kappa_\lambda I_{m\lambda}^+ \tag{6}$$

with the boundary condition of

$$I_{m\lambda}^+(0) = \frac{1-\varepsilon_{uw}}{\pi}\int_{\hat{n}.\hat{s}<0} I_{m\lambda}^-(0)\left|\hat{n}.\hat{s}\right|d\Omega. \tag{7}$$

Due to applying the separation technique, this boundary condition does not include any emission related term.

For the $I_{w\lambda}^+$, the RTE is:

$$\frac{1}{2}\frac{dI_{w\lambda}^+}{dx} = -\kappa_\lambda I_{w\lambda}^+ \tag{8}$$

This equation has only the absorption term. The boundary condition for Eq. (8) is written as:

$$I_{w\lambda}^+(0) = \varepsilon_{uw}\varepsilon_{flame} I_{b\lambda}(T_{uw}) + \frac{1-\varepsilon_{uw}}{\pi}\int_{\hat{n}.\hat{s}<0} I_{w\lambda}^-(0)|\hat{n}.\hat{s}|d\Omega \tag{9}$$

To obtain the RTEs for the separated form of FSCK method, a similar procedure as that of the compact FSCK is followed for

each of the intensities, i.e. $I^+_{m\lambda}$ and $I^+_{w\lambda}$. The change of absorption spectra of hydrocarbon liquid fuels with temperature is negligible [16,17] and therefore can be neglected in deriving the k-distributions [13]. Hence, a k-distribution function is defined by applying the blackbody intensity as the weighting function:

$$f(T,k) = \frac{1}{I_b}\int_0^\infty I_{b\lambda}(T)\delta(k-\kappa_\lambda)d\lambda \tag{10}$$

Multiplying two sides of the Eqs. (6) and (7) with the given delta function in Eq. (10) and integrating over the entire spectrum, the following equations are obtained:

$$\frac{1}{2}\frac{dI^+_{mk}}{dx} = k(f(T,k)I_b - I^+_{mk}) \tag{11}$$

$$I^+_{mk}(0) = \frac{1-\varepsilon_{uw}}{\pi}\int_{\hat{n}.\hat{s}<0} I^-_{mk}(0)\left|\hat{n}.\hat{s}\right|d\Omega \tag{12}$$

where

$$I^+_{mk} = \int_0^\infty I^+_{m\lambda}\delta(k-\kappa_\lambda)d\lambda \tag{13}$$

Similarly, for the Eqs. (8) and (9):

$$\frac{1}{2}\frac{dI^+_{wk}}{dx} = -kI^+_{wk} \tag{14}$$

$$I^+_{wk}(0) = \varepsilon_{uw}\varepsilon_{flame}f(T_{uw},k)I_b(T_{uw}) + \frac{1-\varepsilon_{uw}}{\pi}\int_{\hat{n}.\hat{s}<0} I^-_{wk}(0)\left|\hat{n}.\hat{s}\right|d\Omega \tag{15}$$

where $I^+_{wk}$ is defined as

$$I^+_{wk} = \int_0^\infty I^+_{w\lambda}\delta(k-\kappa_\lambda)d\lambda. \tag{16}$$

$f(T,k)$ is an ill-behaved function due to its fluctuations and singularities [27]. Therefore, a cumulative k-distribution function is defined as [27]:

$$g(T,k) = \int_0^k f(T,k)dk \tag{17}$$

Equation (17) gives a monotonically increasing function for k-distribution. By dividing two sides of Eqs. (11) and (12) with a k-distribution function at a reference temperature, the RTE for medium emission is obtained as

$$\frac{1}{2}\frac{dI^+_{mg}}{dx} = k(a(T,T_{ref,m},g_{ref,m})I_b(T) - I^+_{mg}) \tag{18}$$

where $I^+_{mg}$ is the forward intensity due to medium emission in $g$ space and the parameter $a$ is defined as:

$$a(T,T_{ref,m},g_{ref,m}) = \frac{f(T,k)}{f(T_{ref,m},k)} = \frac{dg(T,k)}{dg_{ref,m}(T_{ref,m},k)} \tag{19}$$

The parameter $T_{ref,m}$ is reference temperature for the RTE of medium emission in the present separated FSCK method. The boundary condition for Eq. (18) is:

$$I^+_{mg}(0) = \frac{1-\varepsilon_{uw}}{\pi}\int_{\hat{n}.\hat{s}<0} I^-_{mg}(0)|\hat{n}.\hat{s}|d\Omega \tag{20}$$

where

$$I^+_{mg} = \frac{I^+_{mk}}{f(T_{ref,m},k)} \tag{21}$$

For the RTE of the boundary's incident intensity, the $f(T,k)$ function is appeared only in the boundary condition equation. Therefore, the wall temperature or an equivalent Planck temperature of the boundary incident intensity has to be used as the reference temperature and consequently the parameter $a$ is eliminated from the RTE . Therefore, the RTE for the irradiation-induced intensity in the separated FSCK method is:

$$\frac{1}{2}\frac{dI^+_{wg}}{dx} = -kI^+_{wg} \tag{22}$$

and its boundary condition is:

$$I^+_{wg}(0) = \varepsilon_{uw}\varepsilon_{flame}I_b(T_{uw}) + \frac{1-\varepsilon_{uw}}{\pi}\int_{\hat{n}.\hat{s}<0} I^-_{wg}(0)|\hat{n}.\hat{s}|d\Omega \tag{23}$$

where

$$I^+_{wg} = \frac{I^+_{wk}}{f(T_{ref,w},k)} \tag{24}$$

Similar to the forward direction, the backward radiation intensity has two components: the intensity originated from the bottom wall ($I^-_{w\lambda}$) and the intensity originated from the medium emission ($I^-_{m\lambda}$). Following the same procedure, these intensities are expressed in $g$ space with the following RTE for the medium emission induced itensity as:

$$\frac{1}{2}\frac{dI^-_{mg}}{dx} = k(a(T,T_{ref,m},g_{ref,m})I_b(T) - I^-_{mg}) \tag{25}$$

with a boundary condition as:

$$I^-_{mg}(L) = \frac{1-\varepsilon_{bw}}{\pi}\int_{\hat{n}.\hat{s}<0} I^+_{mg}(L)|\hat{n}.\hat{s}|d\Omega. \tag{26}$$

For Eqs. (18) and (25), a same reference temperature is applied. For the wall induced intensity in the backward direction, the RTE is:

$$\frac{1}{2}\frac{dI^-_{wg}}{dx} = -kI^-_{wg} \tag{27}$$

with a given boundary condition as:

$$I^-_{wg}(L) = \varepsilon_{bw}I_b(T_{bw}) + \frac{1-\varepsilon_{bw}}{\pi}\int_{\hat{n}.\hat{s}<0} I^+_{wg}(L)|\hat{n}.\hat{s}|d\Omega. \tag{28}$$

Equation (27) has its own reference temperature that is the bottom wall temperature.

Applying the separated FSCK method to model radiation heat transfer in condensed materials allows applying different reference temperatures for the absorption of the boundary radiation intensity and medium emission. It paves the road for high fidelity modeling of both absorption and emission in the condensed materials by the FSCK method. While the look up tables for $a$ and $k$ reported in [13] can be readily used to solve Eqs. (3), (18) and (22) for five liquid fuels considered in the case studies, for clear PMMA, using the high resolution absorption spectra, a look-up table is generated for the temperature range of 300 K to 2000 K with a step of 50 K and is provided in the supplementary materials of the present work.

## 3. Validation case studies

In the validation test cases of the present work, transmissivity and radiative heat source are reported for different modeling options of the compact (original) and the separated FSCK methods. The transmissivity is defined as

$$\tau = \frac{I^+_{out}}{I^+_{in}} \tag{29}$$

where $\tau$ is the transmissivity and parameters $I^+_{out}$ and $I^+_{in}$ represent the outgoing total intensity from each cell along a 1D layer of condensed materials and total incident intensity from the boundary wall facing the source of radiation, respectively. To calculate the total intensity, Gauss-Chebyshev method [28] is applied:

$$I_{m(w)} = \int_0^1 I_{mg(wg)}dg \approx \sum_{i=0}^{n} w_i I_{mg_i(wg_i)} \tag{30}$$

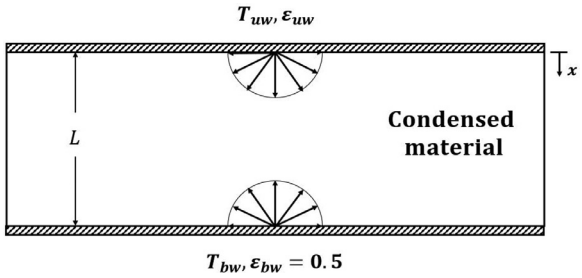


**Fig. 1.** The geometry of the validation test cases.

In the above equation, $n$, $w_i$ and $I_{m(w)g_i}$ are the number of quadrature points (QP), weighting parameter and intensity at each QP. After solving two RTEs of the separated FSCK method, the total intensity is defined as the summation of two intensities as:

$$I = I_m + I_w \tag{31}$$

Solving the RTEs for the forward and backward intensities of two flux method, the forward and backward radiative heat fluxes are given by $(\dot{q}'')^+ = \pi I^+$ and $(\dot{q}'')^- = \pi I^-$, respectively. The new model is not limited to two flux method and is readily applicable to any RTE solvers regardless of their treatment of directional dependency. Finally, the radiative heat source is calculated for each cell as

$$\dot{q}'''_{rad} = \frac{d(\dot{q}'')^+}{dx} + \frac{d(\dot{q}'')^-}{dx} \tag{32}$$

To investigate the effect of different parameters in performance of the separated FSCK method compared to the compact FSCK method, three case studies are introduced in this section. For all of these cases, different modeling options of HR, the compact FSCK, and the separated FSCK methods are applied to solve spectral thermal radiation penetration in the geometry shown in Fig. 1.

Five liquid fuels including decane, ethanol, ethylene glycol, heptane, and toluene as well as clear PMMA are considered as the condensed materials in the case studies. The layer of the fuels as shown in Fig. 1 faces irradiation at its upper boundary from radiation sources with various total (spectrally integrated) radiant power and spectral profiles. To comprehensively investigate the effect of various radiation sources on accuracy of the models, a wide range of temperatures from 500 K to 2000 K is applied in all the case studies.

The first case study applies the estimated value of flame emissivity for a direct flame of the liquid fuels in large pool fires (i.e. 0.4 [14]) and a lower value of 0.05. The flame emissivity of 0.4 represents an extreme scenario for the high incident intensity at the material surface. In real cases, the source of the incident intensity can be an inclined flame or other hot sources in surroundings where a view factor should be considered in addition to the flame emissivity that weakens the incident intensity at the fuel surface. This kind of conditions is mimicked in the first case study by defining the value of 0.05 for the flame emissivity. To simplify the calculations, emissivity of the upper layer is assumed to be 1. The layer thickness in the first case study was 8 mm for the liquids and 10 mm for PMMA.

To check sensitivity of the modeling predictions to thickness of the layers, in the second case study, two different thicknesses are considered for the layer of the condensed materials as introduced in Table 1.

In the first two case studies, a constant flame emissivity for the upper surface has been considered for all the studied Planck temperatures representing the boundary incident intensities. Considering the constant flame emissivity, the relative importance of the medium emission compared to the irradiation from the radiation source is small for the high temperature radiation sources and is larger for the lower temperature radiation sources. To investigate the performance of different models for the cases in which the relative importance of the medium emission compared to irradiation from the source is kept constant, the third case study applies the variable flame emissivity for the upper wall to keep the incident radiation energy nearly constant at the material surface. For this case study, the flame emissivity is calculated for different upper wall temperatures by the following equation:

$$\varepsilon_{flame} = 0.4\left(\frac{500}{T_{uw}}\right)^4 \tag{33}$$

The settings of three different test cases for the modeled geometry shown in Fig. 1 are summarized in Table 1.

In the present research, the flame irradiation has been assumed to have a scaled Planck distribution using the considered flame emissivities. To include more realistic flame intensity profile, a non-gray wall can be applied by considering spectral emissivity (instead of the current gray constant emissivity) in Eqs. (2) and (9). The presented method in [29] can be then applied to give the boundary condition needed for Eqs. (3) and (22). This is a part of our ongoing research and will be included in our future publications.

To eliminate the effect of the quadrature scheme used in numerical integration (Eq. (30)) on the accuracy of the FSCK models, all the FSCK calculations are done for 32 QP which is the finest quadrature scheme for which the FSCK model parameters have been obtained. The boundary condition of the bottom of the condensed materials is fixed with a wall emissivity of 0.5 and a temperature obtained by the given temperature profiles in Tables 2 and 3.

In agreement with the experimental observations [30,31], for all the considered case studies, a nonlinear temperature profile is considered for temperature in the layer of the condensed materials. For the liquid fuels with thickness of 40 mm, the nonlinear temperature profile is introduced in Table 2. For the layer thickness of 8 mm, the applied nonlinear temperature profile given in [13] is used.

**Table 1**
Summary of settings of the different case studies.

| | $\varepsilon_{flame}$ | $T_{uw}(K)$ | $L(mm)$ | Number of QP |
|---|---|---|---|---|
| Case 1 | 0.4, 0.05 | 500-2000 | 8,10* | 32 |
| Case 2 | 0.4 | 500-2000 | 8, 40, 10*, 25* | 32 |
| Case 3 | Equation (27) | 500-2000 | 8, 10* | 32 |

*These thicknesses are applied for the clear PMMA while the others are applied for liquid fuels.

**Table 2**
The coefficients of the considered temperature profiles of the liquid fuels with thickness of 40 mm: $T(x) = a.exp(-b.x) - c.exp(-d.x)$

| Fuel | $a$ | $b$ | $c$ | $d$ |
|---|---|---|---|---|
| Decane | 574.5 | 16.12 | 127.3 | 111.5 |
| Ethanol | 379.9 | 5.895 | 28.37 | 145.5 |
| Ethylene glycol | 823.3 | 23.22 | 353.1 | 65.99 |
| Heptane | 445.7 | 9.651 | 74.11 | 80.57 |
| Toluene | 614 | 15.13 | 230.3 | 46.89 |

**Table 3**
The coefficients of the considered temperature profile for two different thicknesses of clear PMMA: $T(x) = a.exp(-b.x) + c.exp(d.x)$

| $L(mm)$ | $a$ | $b$ | $c$ | $d$ |
|---|---|---|---|---|
| 25 | 377.6 | 398.4 | 290.4 | 1.584 |
| 10 | 468.9 | 273.2 | 189.3 | 38.54 |

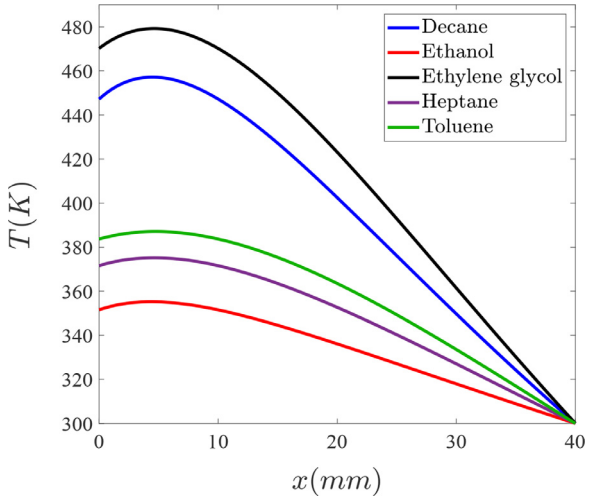


**Fig. 2.** The considered temperature profiles within liquid fuels with layer thickness of 40 mm.

The considered temperature profiles for the 40 *mm* layer of liquid fuels are shown in Fig. 2.

For PMMA, two thicknesses commonly used in cone calorimeter experiments (i.e. 10 and 25 mm) are applied with the temperature profiles given based on experimental observations [32] in Table 3.

The considered temperature profiles of the PMMA layers given in Table 3 are shown in Fig. 3.

## 4. Results and discussions

The results of the case studies are presented in the form of averaged relative errors of radiative heat source and transmissivity. The various temperatures of radiation source with a step of 100 K within the temperature range listed in Table 1 are considered in the calculations. Due to strong radiative absorption of the condensed materials, most parts of the spectral incident intensity is absorbed within a thin layer in order of a few millimeters near the top boundary. In addition, considering the temperature profile of the liquids and PMMA, this part of the materials has higher medium emission. This thin layer is the most important part of the medium in which thermal radiation should be accurately modeled. Hence, to consider a higher weight for this layers in calculations of average errors of the models, a weighted arithmetic mean relative errors is introduced as:

$$\delta\dot{q}''' = \sum_{i=0}^{n} w'_i . \frac{|\dot{q}'''_{HR,i} - \dot{q}'''_{FSCK,i}|}{|\dot{q}'''_{HR,i}|} \times 100 \tag{34}$$

where $w'_i$ is the weight parameter and is calculated from:

$$w'_i = \frac{|\dot{q}'''_{HR,i}|}{\sum_{i=1}^{n} |\dot{q}'''_{HR,i}|} \tag{35}$$

For the transmissivity, the relative error is calculated using the following equation:

$$\delta\tau = \sum_{i=1}^{n} w''_i . \frac{|\tau_{HR,i} - \tau_{FSCK,i}|}{\tau_{HR,i}} \times 100 \tag{36}$$

where $w''_i$ is the weight parameter for relative error of the transmissivity and is given as:

$$w''_i = \frac{(\dot{q}''_{HR,i})^+}{\sum_{i=1}^{n} (\dot{q}''_{HR,i})^+} \tag{37}$$

### 4.1. Mesh independence study

To insure mesh independence of the simulation results and selecting an appropriate number of grids in each thickness, several simulations were performed for the 40 mm layer of toluene using the flame emissivity of 0.4 and the upper wall temperature of 1000 K. The results of the simulations are shown in Fig. 4 which confirms the 200 grids as an optimal computational grid structure. Using larger number of computational grids does not significantly alter the results of the FSCK models.

In the case of PMMA, similar simulations were done for the thickness of 25 mm using the flame emissivity of 0.4 and the upper wall temperature of 1000 K. Fig. 5 shows that for the 25 mm layer of PMMA, using of 125 grids leads to the mesh independent results.

For the 8 mm layer of liquid fuels and 10 mm layer of PMMA, same grid size with [13] is applied in the simulations.

### 4.2. Effect of flame emissivity

The first case study addresses the effect of the flame emissivity on accuracy of two different FSCK methods. For this case study, two values of 0.4 and 0.05 have been applied for the flame emissivity. Due to the closeness of their boiling temperatures, the results for decane and ethylene glycol have some similarities and therefore are given in a same figure. As shown in Fig. 6, for lower flame emissivity, the difference between the results of the two methods increases due to the higher relative importance of liquid emission. The liquid emission can not be estimated accurately with applying the Planck temperature of the boundary incident intensity as the reference temperature in the original (compact)

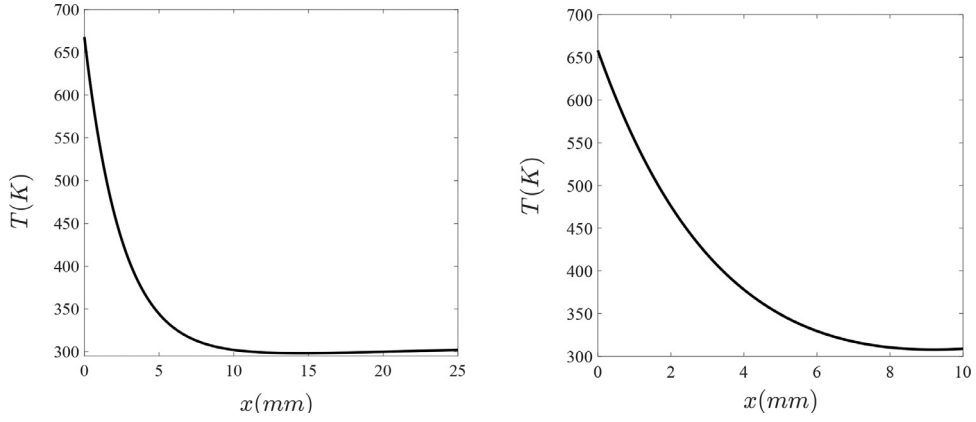


**Fig. 3.** The considered temperature profiles within clear PMMA with layer thickness of: left) 25 mm, and right) 10 mm.

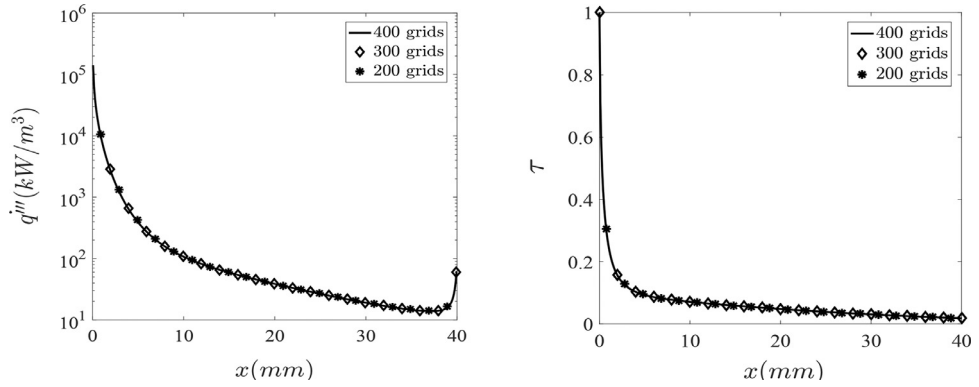


**Fig. 4.** Mesh independence study; Radiative heat source (left) and transmissivity (right) of the 40 mm layer of toluene with the conditions of the first case study.

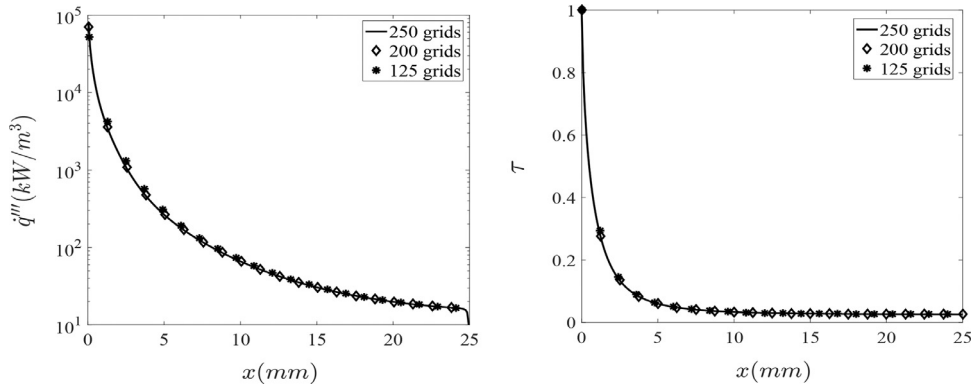


**Fig. 5.** Mesh independency study; Radiative heat source (left) and transmissivity (right) of the 25 mm layer of clear PMMA with the conditions of the first case study.

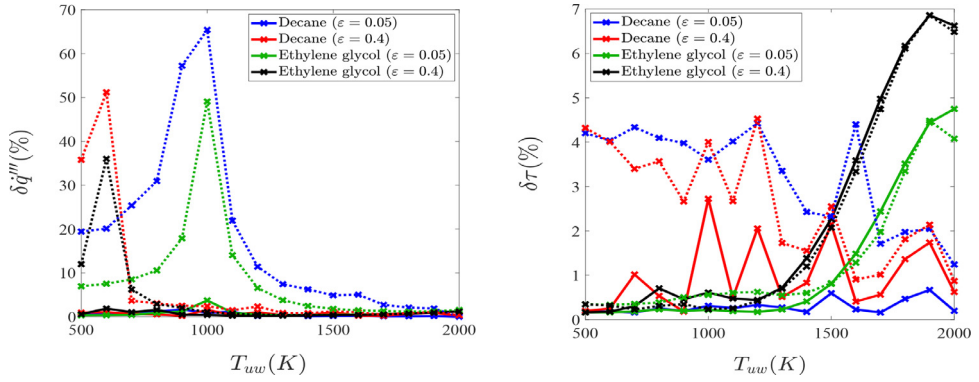


**Fig. 6.** The averaged relative error of radiative heat source (left) and transmissivity (right) for decane and ethylene glycol for two different flame emissivities. Solid-line: The separated FSCK method and dotted-line: The compact FSCK method

form of the FSCK method. Therefore, the higher relative importance of the liquid emission increases the inaccuracy of the original FSCK method. This issue is well tackled by the separated FSCK method in which the liquid emission is modeled with its own RTE solution and reference temperature. For the cases with smaller flame emissivity, the differences between the predictions of two FSCK methods extends toward the cases with stronger radiation source.

By applying the lower flame emissivity for the incident intensity, the emission of ethanol shows its effect on the results. According to Fig. 7, for the flame emissivity of 0.05, the separated FSCK improves the results for the cases with the source temperature of up to 1200 K while for the flame emissivity of 0.4 the predictions of two FSCK methods are very close for the source temperatures higher than 600 K. This reveals the effect of the relative importance of the incident intensity at the boundary and liquid emission. When the relative importance of the liquid emission is negligible, the results of the two methods are close.

Similar observations are seen for heptane and toluene as shown Fig. 8. By decreasing the flame emissivity, difference between the results of two methods increases especially in the cases with the higher source temperatures. By applying the flame emissivity of 0.05, the separated FSCK method improves the results of heptane and toluene for the source temperature up to 1400 K while this temperature for the flame emissivity of 0.4 is 800 K.

For the PMMA, the difference in the results of two FSCK methods is more highlighted than that of the liquid fuels. Fig. 9 shows that using the separated FSCK method improves the accuracy of the predicted radiative heat source even for the cases with higher wall temperatures up to 2000 K. The lower emissivity increases the difference between the results of two FSCK methods even more. Therefore, in comparison to the liquid fuels, the separated FSCK

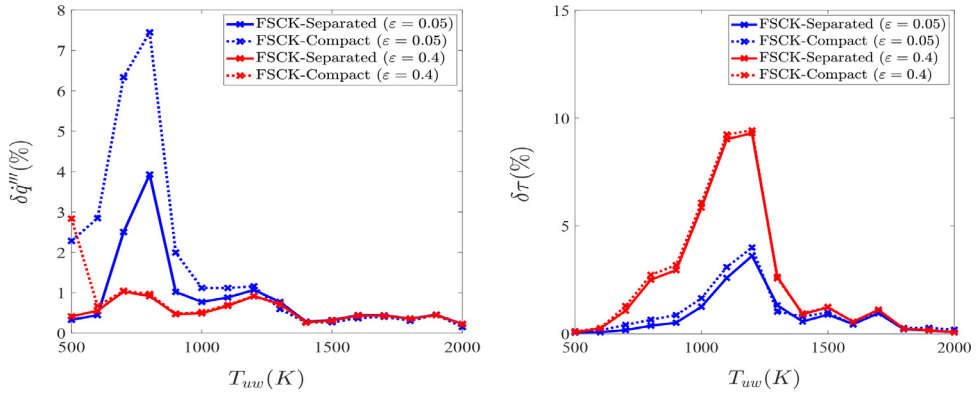


**Fig. 7.** The averaged relative error of radiative heat source (left) and transmissivity (right) for ethanol with using of two different flame emissivities.

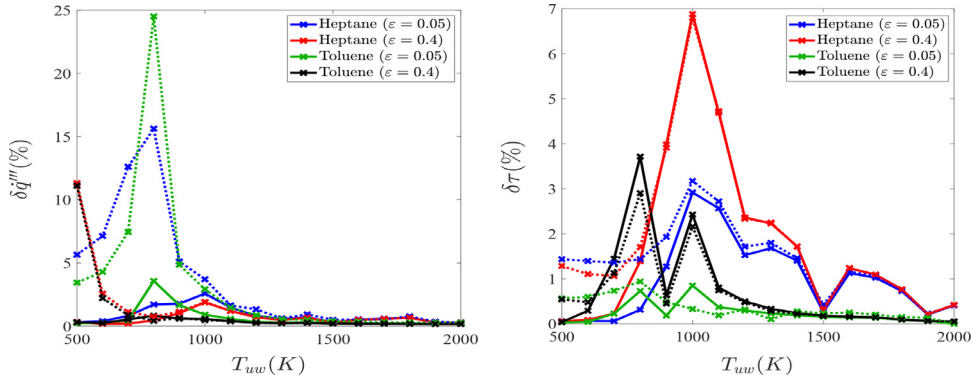


**Fig. 8.** The averaged relative error of radiative heat source (left) and transmissivity (right) for heptane and toluene with using of two different flame emissivities. Solid-line: The separated FSCK method and dotted-line: The compact FSCK method

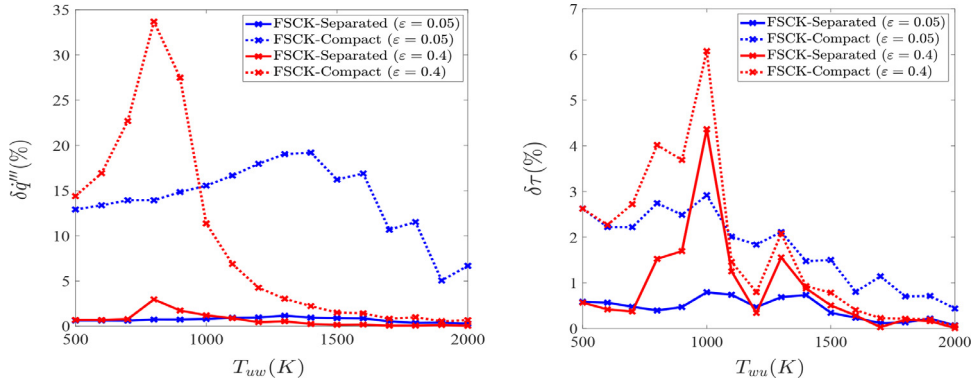


**Fig. 9.** The averaged relative error of radiative heat source (left) and transmissivity (right) for PMMA with using of two different flame emissivities.

method brings more advantages for PMMA due to its higher level of medium emission.

### 4.3. The effect of the reference temperature for the medium emission

While it is obvious that the Planck equivalent temperature of the irradiation at the boundary should be used as the reference temperature in solution of irradiation-induced intensity (Eq. (22)–(24)), in this section we investigate which choice of the reference temperature gives the best accuracy for the emission induced intensity ($I_{m\lambda}$ and Eq. (18)) in the separated FSCK method. The volume-weighted averaged temperature and Planck mean temperature are reported as the suitable options for the FSCK in gaseous media where emission is usually dominating. To find the best choice for the condensed materials, some simulations were performed for the 40mm layer of ethylene glycol assuming no boundary irradiation at the upper wall. Among the considered liquid fuels, ethylene glycol has the highest boiling temperature and in the thickest layer of this fuel, one can anticipate the largest difference between the predictions of the separated FSCK method using the maximum temperature of the medium and the volume-averaged temperature as the reference temperature. Therefore, we decided to apply this liquid fuel to study different choices of reference temperature. Fig. 10 shows the heat source and heat flux calculated by the separated FSCK method for a 40 mm layer of ethylene glycol.

Fig. 10 confirms that applying the maximum temperature of the medium and the volume-averaged temperature results in identical predictions of radiative heat source and heat flux. Therefore, each of these two reference temperatures can be selected for the solution of the emission induced intensity in the separated FSCK method (Eqs. (18)–(20)). However, in this research the volume-averaged temperature is used as the reference temperature.

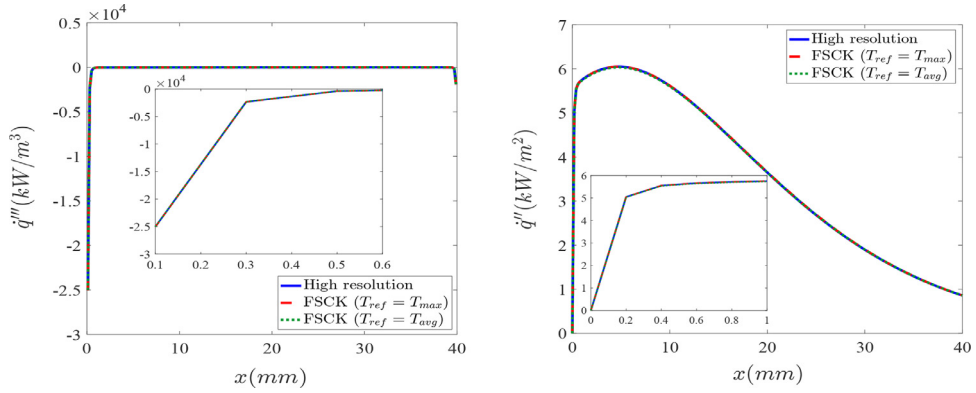


**Fig. 10.** Comparison of predictions of the separated FSCK method for the radiative heat source (left) and heat flux (right) of a 40 mm ethylene glycol layer using different reference temperatures compared to the results of the high resolution calculations.

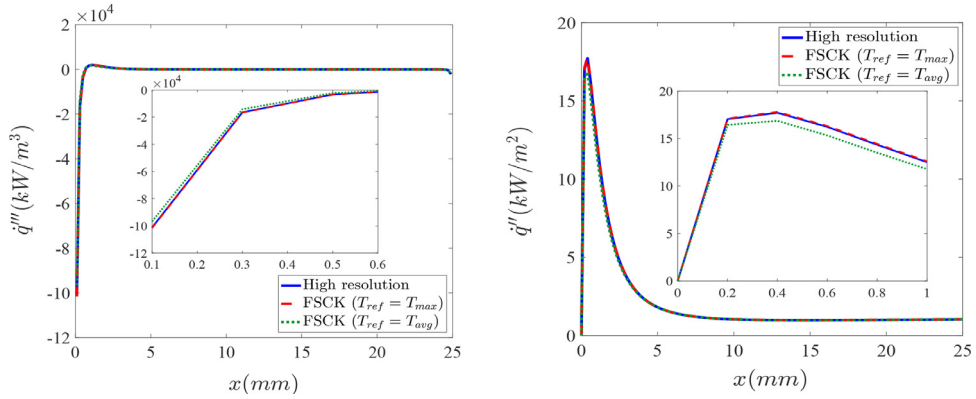


**Fig. 11.** Comparison of predictions of the separated FSCK method for the radiative heat source (left) and heat flux (right) of a 25 mm layer of clear PMMA using different reference temperatures compared to the results of the high resolution calculations.

The convective motions do not play a role in heat transfer within the solids. Hence, for the solids with low conductivity like PMMA, temperature profile shows a sharp increase within the thin layer below the material surface especially for high irradiation at the boundary. Due to this form of temperature profile, the maximum temperature of the solids has a significant difference with the volume-averaged or Planck-mean temperatures. Therefore, using these temperatures as the reference temperature in the simulations may affect the accuracy. To investigate this, some simulations were performed on a 25 mm thickness of the PMMA and the results are shown in Fig. 11.

As Fig. 11 shows, applying the maximum temperature of the medium as the reference temperature in PMMA gives the highest accuracy.

### 4.4. Effect of material thickness

The first case study was for one thickness of liquid fuels and PMMA. In the second case study the sensitivity of the results of two FSCK methods with respect to thickness of the fuel layer is investigated. For this case study, two different thicknesses of 8 and 40 mm have been considered for the liquid fuels. The results of decane and ethylene glycol are given in Fig. 12. While the accuracy of the radiative source term calculated by the separated FSCK method is high, it is not that good for transmissivity especially for the thicker layer with high source temperatures. Nonetheless it is not worse than that of the compact FSCK method. By increasing the thickness, most part of liquid layer receives highly reshaped incident intensity that cannot be accurately correlated by the K-distribution obtained from the boundary temperature used for RTE solution of the wall induced intensity (i.e. Eqs. (22)–(24)).

Within cold gaseous media the correlated-k overpredicts the medium absorption [33]. Similar phenomenon happens in applying the FSCK method in condensed materials. In the condensed materials with strong absorption, various spectral regions of incident intensity are absorbed in different thicknesses mostly close to the material surface. Therefore, for the deeper layers of the condensed materials, many parts of the absorption spectra gradually lose their role in absorbing the wall irradiation. However, the calculated k-distribution with the wall's irradiation cannot simulate this effect of strong absorption for deeper layers that results in the so-called "absorption overprediction". For the thicker layers of the condensed materials, this effect of absorption overprediction is stronger.

Similarly by increasing the thickness of the fuel layer of ethanol, the inaccuracy increases as shown in Fig. 13. For ethanol, boiling temperature is lower (i.e. 351.53 K), therefore the separated FSCK method improves the results for low temperature of the upper wall only. There is a peak of inaccuracy seen for the case with the boundary temperature of 1200K. It is because of the form of the absorption spectra of this liquid which has strong absorption in the same spectral region as the peak of Planck spectral intensity of $T_{wu} = 1200\,K$.

For heptane and toluene, the difference between the results of two FSCK methods is smaller. For these two liquid fuels as shown in Fig. 14, there are two peaks of inaccuracy at 1000, and 800 K for heptane and toluene, respectively, which are due to the stronger absorption of these liquids at these temperatures. Moreover, similar to etylene glycol and ethanol, for these two liquid fuels also the stronger absorption increases the relative error for the thickness of 40 mm. The averaged relative error of the radiative heat source is lower than 3% using the separated FSCK method for both liquids.

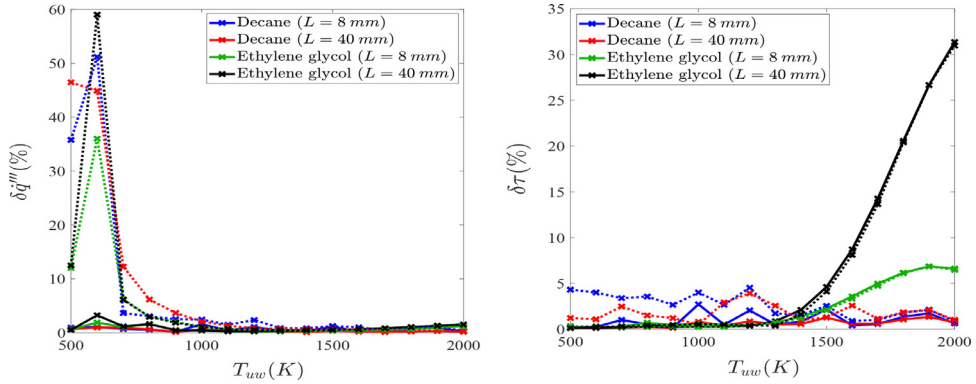


**Fig. 12.** The averaged relative error of radiative heat source (left) and transmissivity (right) for different thicknesses of decane and ethylene glycol layers. The solid lines represent the separated FSCK method and the dotted lines represent the compact FSCK method.

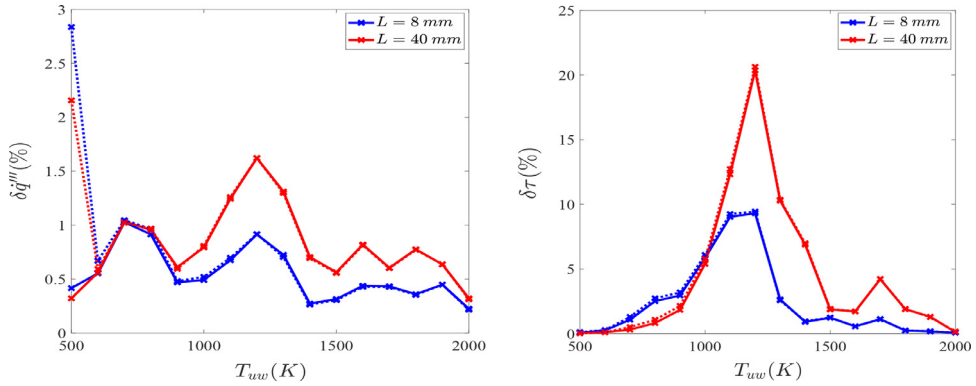


**Fig. 13.** The averaged relative error of radiative heat source (left) and transmissivity (right) for different thicknesses of the ethanol layer. The solid lines represent the separated FSCK method and the dotted lines represent the compact FSCK method.

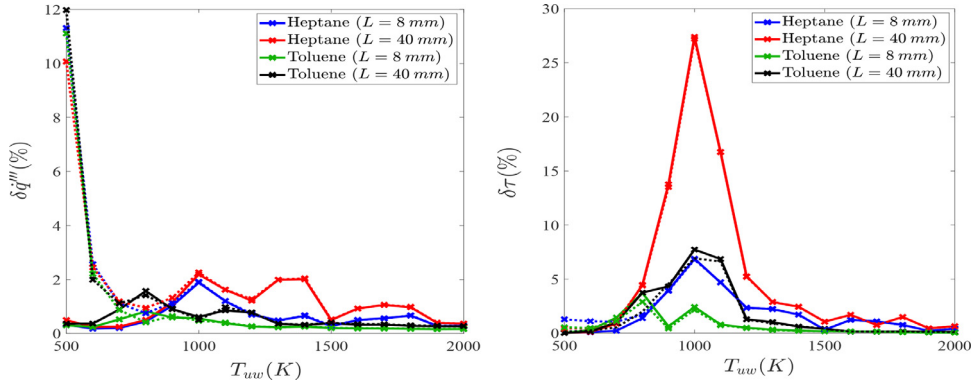


**Fig. 14.** The averaged relative error of radiative heat source (left) and transmissivity (right) for different thicknesses of heptane and toluene layers. The solid lines represent the separated FSCK method and the dotted lines represent the compact FSCK method.

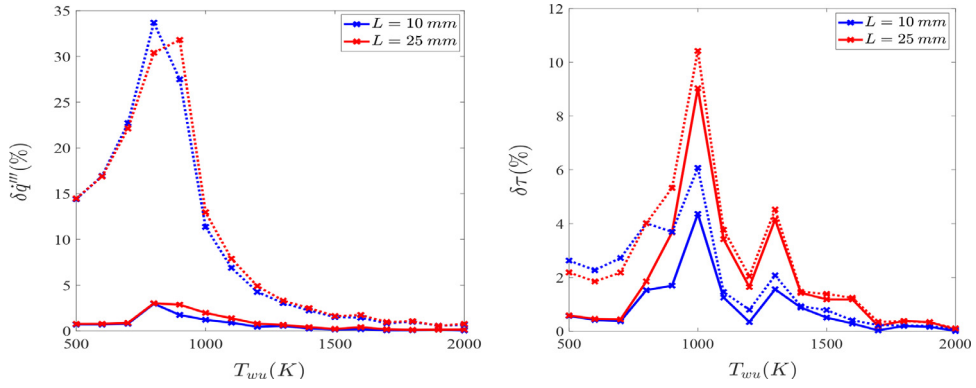


**Fig. 15.** The averaged relative error of radiative heat source (left) and transmissivity (right) for different thicknesses of PMMA layer. The solid lines represent the separated FSCK method and the dotted lines represent the compact FSCK method.

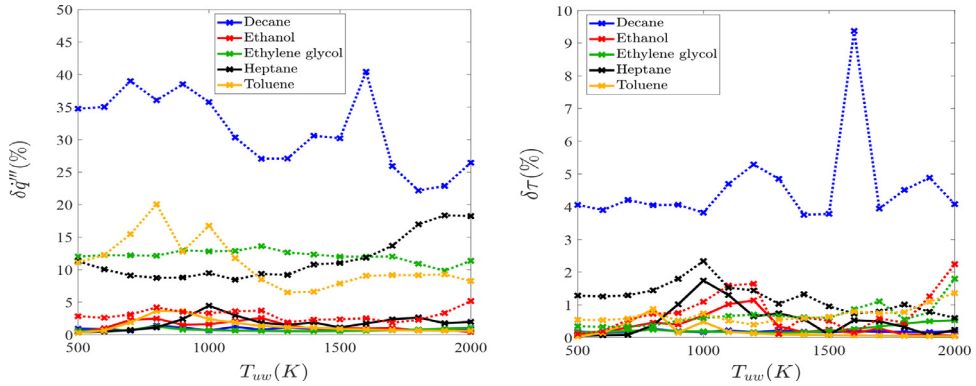


**Fig. 16.** The averaged relative error of radiative heat source (left) and transmissivity (right) for different liquid fuels with constant energy of the boundary's irradiation at different upper wall temperatures. The solid lines represent the separated FSCK method and the dotted lines represent the compact FSCK method.

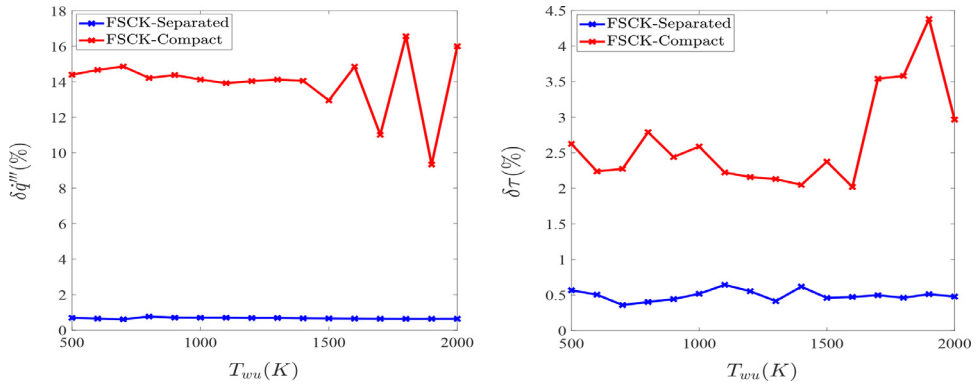


**Fig. 17.** The averaged relative error of radiative heat source (left) and transmissivity (right) for PMMA with a constant energy of incident radiation at different boundary temperatures.

To check the sensitivity of the models to the fuel layer thickness, two sample thicknesses of 10 mm and 25 mm of PMMA were modeled and the results are shown in Fig. 15. Similar to the liquid fuels, the separated FSCK method provides more accurate radiative source term than the compact FSCK method. Similarly, the averaged relative error of transmissivity for the PMMA increases with the sample thickness.

### 4.5. Effect of spectral distribution of the boundary irradiation

To study how the spectral form of the irradiation reaching from a source to the fuel layer may affect the accuracy of two FSCK methods, there was a need for some cases with the same total radiating power reaching the fuel layer but different spectral forms. Moreover, the relative importance of the liquid emission and irradiation at the boundary should be the same for all the cases to provide a fair sensible ground for studying the effect of spectral form of irradiation at the boundary. This is done by changing the value of the flame emissivity using the Eq. (33) in the third case study. The results of the third case study for different liquid fuels are presented in Fig. 16. As seen, by keeping the relative importance of the medium emission at a same level for all the source temperatures, the separated FSCK method constantly provides better results than the compact FSCK method. The lowest improvement is observed for ethanol due to its weaker emission.

The presented results in Fig. 16 reveal the effect of the shape of absorption spectrum for different liquid fuels. As explained before, absorption overprediction with both FSCK methods causes an error in estimating radiative heat source and transmissivity. However, for different source temperatures, different parts of the absorption spectra are important. This changes the amount of absorption overprediction in different spectral forms of the boundary's irradiation. For the considered liquid fuels, the values and fluctuations of the averaged relative error are different due to the shape of spectrum for each liquid fuel.

For PMMA, as shown in Fig. 17 the results of the third case study show an excellent accuracy of the separated FSCK method. In this case, the averaged relative errors are less than 1% for both radiative heat source and transmissivity. Due to the shape of the absorption spectrum of PMMA, severe peaks are not observed in the relative error diagrams as will be discussed in more details in the next section.

### 4.6. Analysis of the simulation errors

The given results of the ethanol, heptane, and toluene showed that there are some peaks in the averaged relative error diagrams at the temperatures of 800, 1000, and 1200 K. To explain these peaks, the spectra of the blackbody radiation intensities and the absorption coefficient of the fuels are plotted in Fig. 18. In the above mentioned inaccuracy peaks of the methods, the peak region of the blackbody intensities of the boundary temperatures overlap with the peak region of the absorption coefficient spectra. With high values of absorption coefficient, almost all part of the boundary's irradiation is absorbed within a few millimeters near to the surface and the spectrum of the incident intensity is highly reshaped at the lower parts of the liquids. In this case, higher absorption overprediction happens with applying the FSCK method that increases the averaged relative error. For other source temperatures that their peak region have not substantial overlap with the peak regions of the absorption coefficient spectra, the role of high absorption values is less significant. Therefore, the amount of

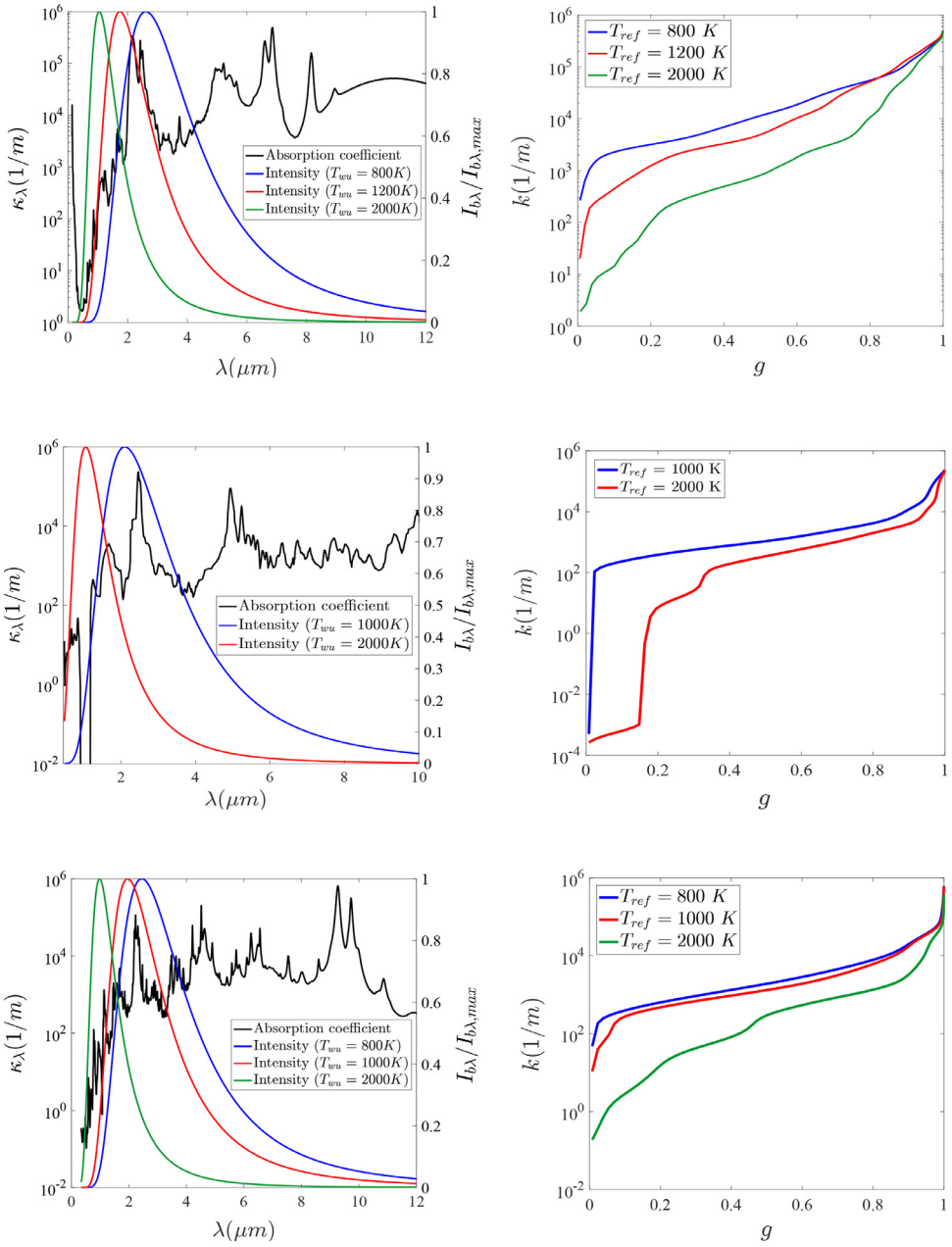


**Fig. 18.** The spectra of absorption coefficient and blackbody intensity (right) and the diagrams of k-g distributions for the same reference temperatures (left): Ethanol (up), heptane (middle), and toluene (bottom).

the absorption over-predictions is smaller. The diagrams of the k-distributions for the temperatures of 800, 1000, and 1200 K, together with 2000 K shown in Fig. 18 confirm this conclusion. At the temperature of 2000 K, due to the lower absorption, the results are very accurate.

### 4.7. Effect of the quadrature scheme

All the presented results for the different case studies were obtained by 32 QP. However, performing simulations with such a large number of QP is computationally expensive for engineering applications. To investigate the accuracy of the methods with the lower numbers of QP, the averaged and maximum values of the averaged relative errors for heat source and transmissivity at various boundary temperatures are presented in Table 4 for 32 and 8 QPs.

Table 4 shows higher inaccuracy for transmissivity compared to the radiative heat source. Due to the difference in the defined weighting parameters in calculation of the relative errors for transmissivity, the lower layers of the fuels have higher weights causing higher averaged relative errors. The highest value of the given maximum relative errors (i.e. $(\delta\tau)_{max}$) for ethanol is due to its higher absorption compared to other fuels. Using 8 QP increases the averaged relative error for radiative heat source compared to 32 QP by a factor of 3 to 6, but it still remains lower than 5%. Depending on the expected simulation accuracy, it can be considered as an option for engineering calculations to reduce the computational time. The simulations were performed using 4 QPs as well and both FSCK methods provided reasonable accuracy in order of 10% for radiative heat source. However, using the smaller number of quadrature points makes the inaccuracy of numerical integration to mask the advantages of better physical modeling offered by the

**Table 4**
The average and maximum values of the averaged relative errors of the heat source and transmissivity in the given temperature range of the upper wall for different fuels

| Fuel | $(\delta \dot{q}''')_{avg}(\%)$ | | $(\delta \dot{q}''')_{max}(\%)$ | | $(\delta \tau)_{avg}(\%)$ | | $(\delta \tau)_{max}(\%)$ | |
|---|---|---|---|---|---|---|---|---|
| | 8 QP | 32 QP | 8 QP | 32 QP | 8 QP | 32 QP | 8 QP | 32 QP |
| Decane | 1.56 | 0.67 | 3.47 | 1.59 | 3.16 | 0.98 | 9.32 | 2.72 |
| Ethanol | 2.69 | 0.54 | 4.18 | 1.03 | 11.28 | 2.37 | 26.46 | 9.31 |
| Ethylene glycol | 2.07 | 0.72 | 4.63 | 1.90 | 6.48 | 2.25 | 16.50 | 6.86 |
| Heptane | 2.99 | 0.60 | 7.07 | 1.88 | 7.79 | 1.73 | 19.65 | 6.88 |
| Toluene | 2.23 | 0.33 | 3.76 | 0.59 | 4.45 | 0.69 | 18.22 | 3.71 |
| Clear PMMA | 4.01 | 0.67 | 13.27 | 2.96 | 5.53 | 0.89 | 15.53 | 4.36 |

separated FSCK method and therefore the overall accuracy of both approaches are in a similar level when applying low number of QPs such as 4.

## 5. Conclusion and remarks

The FSCK method for solving spectral radiation penetration into condensed materials have been modified by separating the RTE solutions of boundary's irradiation from a radiation source or flame and medium emission. It provides more accurate and physically sound way to model medium emission in the cases where it is in a comparable magnitude with the boundary's irradiation. Applying the novel separated FSCK method enables solving two RTEs for the medium emission and the boundary's incident intensity with their own reference temperatures. Investigating the solution of RTE of the medium emission in the separated FSCK method showed that in the case of clear PMMA, the maximum temperature of the medium should be selected as the reference temperature while for the liquid fuels, the reference temperature can be either the volume-averaged temperature or maximum temperature of the medium.

To demonstrate the privileges of the novel separated FSCK method in comparison with the original compact FSCK method, three different case studies have been defined and simulated. The results are presented in a form of a weighted arithmetic mean relative error of radiative heat source and transmissivity within the temperature range of 500 K to 2000 K for the upper wall. The main conclusions of the case studies are as follows:

- In all the considered case studies, the separated FSCK method performed better than the original compact FSCK method.
- The first case study proved the accuracy improvements offered by the separated FSCK method especially for the high source temperatures with small flame emissivity or in the presence of the lower view factors.
- The sensitivity analysis of the separated FSCK method with respect to the fuel thickness in the second case study showed the higher averaged relative error in the cases with thicker layers of the condensed materials. It is explained by strong absorption of the first layers underneath the surface which causes rapid change in the intensity spectra of the boundary's irradiation. Consequently the k-distribution obtained by the boundary temperature as the reference temperature cannot accurately model the absorption of the material further away from the boundary.
- Applying the constant level of incident intensity in the third case study, the separated FSCK method enhanced the accuracy for all the upper wall temperatures. The third case study addressed how conformity of the absorption spectra of the condensed materials and the Planck intensity profile affects accuracy of the separated FSCK method. The overlap between the peak region of the incident intensity and peak region of absorption coefficient spectra strengthens the absorption overprediction by the FSCK method.
- While the advantages of the separated FSCK method are clearly seen in the simulations with 8 QP and larger, the accuracy of the models with the lower QPs is more affected by the inaccuracy of numerical integration that masks the improvement made by the separated FSCK method.

## Declaration of Competing Interest

Reffering to manuscript entitled as "Improving the modeling of spectral radiation penetration into the condensed materials with the separated full spectrum correlated-k method" submitted to International Journal of Heat and Mass Transfer, we wish to confirm that there are no known conflicts of interest associated with this publication and there has been no significant financial support for this work that could have influenced its outcome. We confirm that the manuscript has been read and approved by all named authors and that there are no other persons who satisfied the criteria for authorship but are not listed. We further confirm that the order of authors listed in the manuscript has been approved by all of us. We confirm that we have given due consideration to the protection of intellectual property associated with this work and that there are no impediments to publication, including the timing of publication, with respect to intellectual property. In so doing we confirm that we have followed the regulations of our institutions concerning intellectual property. We understand that the Corresponding Author is the sole contact for the Editorial process (including Editorial Manager and direct communications with the office). He is responsible for communicating with the other authors about progress, submissions of revisions and final approval of proofs. We confirm that we have provided a current, correct email address which is accessible by the Corresponding Author.

## CRediT authorship contribution statement

**Farid Alinejad:** Conceptualization, Methodology, Software, Validation, Formal analysis, Investigation, Resources, Data curation, Writing - original draft, Visualization. **Hadi Bordbar:** Conceptualization, Methodology, Resources, Writing - review & editing, Investigation, Supervision, Project administration. **Simo Hostikka:** Conceptualization, Methodology, Writing - review & editing, Supervision, Project administration, Funding acquisition.

## Acknowledgements

The authors greatly acknowledge the support of the Academy of Finland under grant no. 314487 and the Finnish Fire Protection Fund (Palosuojelurahasto). The kind help of Professor Pascal Boulet from University of Lorraine, France in providing the spectral data of clear PMMA is greatly acknowledged.

## Supplementary materials

Supplementary material associated with this article can be found, in the online version, at doi:10.1016/j.ijheatmasstransfer.2021.121448.

## References


[1] M.H. Bordbar, P. Zamankhan, Dynamical states of bubbling in vertically vibrated granular materials. Part I: collective processes, Commun. Nonlin. Sci. Numer.Simul. 12 (3) (2007) 254–272, doi:10.1016/j.cnsns.2005.04.001.

[2] M.H. Bordbar, P. Zamankhan, Dynamical states of bubbling in vertical vibrated granular materials. Part II: theoretical analysis and simulations, Commun. Nonlin. Sci. Numer.Simul. 12 (3) (2007) 273–299, doi:10.1016/j.cnsns.2005.03.008.

[3] M.H. Bordbar, T. Hyppnen, Multiscale numerical simulation of radiation heat transfer in participating media, Heat Transf. Eng. 34 (1) (2013) 54–69, doi:10.1080/01457632.2013.695210.

[4] M.H. Bordbar, T. Hyppnen, The correlation based zonal method and its application to the back pass channel of oxy/air-fired CFB boiler, Appl. Therm. Eng. 78 (2015) 351–363, doi:10.1016/j.applthermaleng.2014.12.046.

[5] M.F. Modest, The weighted-sum-of-gray-gases model for arbitrary solution methods in radiative transfer, J. Heat Transf. 113 (3) (1991) 650–656, doi:10.1115/1.2910614.

[6] M.H. Bordbar, G. Wecel, T. Hyppänen, A line by line based weighted sum of gray gases model for inhomogeneous CO2-H2O mixture in oxy-fired combustion, Combust. Flame 161 (9) (2014) 2435–2445, doi:10.1016/j.combustflame.2014.03.013.

[7] H. Bordbar, G.C. Fraga, S. Hostikka, An extended weighted-sum-of-gray-gases model to account for all CO2-H2O molar fraction ratios in thermal radiation, Int. Commun. Heat Mass Transf. 110 (2020) 104400, doi:10.1016/j.icheatmasstransfer.2019.104400.

[8] M.K. Denison, B.W. Webb, Spectral line-based weighted-sum-of-gray-gases model for arbitrary RTE solvers, J. Heat Transf. 115 (4) (1993), doi:10.1115/1.2911354.

[9] V.P. Solovjov, F. Andre, D. Lemonnier, B.W. Webb, The generalized SLW model, J. Phys. Conf. Ser. 676 (2016) 012022.

[10] M.F. Modest, H. Zhang, The full-spectrum correlated-k distribution and its relationship to the weighted-sum-of-gray-gases method, ASME-PUBLICATIONS-HTD 366 (2000) 75–84.

[11] M.F. Modest, H. Zhang, The full-spectrum correlated-k distribution for thermal radiation from molecular gas-particulate mixtures, J. Heat Transf. 124 (1) (2002) 30–38, doi:10.1115/1.1418697.

[12] T. Isojärvi, H. Bordbar, S. Hostikka, Spectrally resolved calculation of thermal radiation penetration into liquid n-heptane in pool fires, Int. J. Heat Mass Transf. 127 (2018) 1101–1109, doi:10.1016/j.ijheatmasstransfer.2018.08.108.

[13] F. Alinejad, H. Bordbar, S. Hostikka, Development of full spectrum correlated k-model for spectral radiation penetration within liquid fuels, Int. J. Heat Mass Transf. 158 (2020) 119990, doi:10.1016/j.ijheatmasstransfer.2020.119990.

[14] J.M. Suo-Anttila, T.K. Blanchat, A.J. Ricks, A.L. Brown, Characterization of thermal radiation spectra in 2 m pool fires, Proc. Combust. Inst. 32 (2) (2009) 2567–2574, doi:10.1016/j.proci.2008.06.044.

[15] V.P. Solovjov, B.W. Webb, F. Andre, The rank correlated FSK model for prediction of gas radiation in non-uniform media, and its relationship to the rank correlated SLW model, J. Quant. Spectrosc. Radiat. Transf. 214 (2018) 120–132.

[16] C.C. Wang, J.Y. Tan, C.Y. Jing, L.H. Liu, Temperature-dependent optical constants of liquid isopropanol, n-butanol, and n-decane, Appl. Opt. 57 (12) (2018) 3003–3011, doi:10.1364/AO.57.003003.

[17] Q. Ai, M. Liu, F. Sun, C. Liu, X. Xia, Near infrared spectral radiation properties of different liquid hydrocarbon fuels, J. Near Infrared Spectrosc. 26 (1) (2018) 5–15.

[18] F. Alinejad, H. Bordbar, S. Hostikka, Enc-2020-0599 sensitivity analysis for the temperature of incident intensity in applying fsck method for liquid fuels, 18th Brazilian Congress of Thermal Sciences and Engineering, 2020. https://www.sistema.abcm.org.br/articleFiles/download/28646.

[19] D.B. Olfe, A modification of the differential approximation for radiative transfer, AIAA J. 5 (4) (1967) 638–643, doi:10.2514/3.4041.

[20] M.F. Modest, Modified differential approximation for radiative transfer in general three-dimensional media, J. Thermophys. Heat Transf. 3 (3) (1989) 283–288, doi:10.2514/3.28773.

[21] M.A. Ramankutty, A.L. Crosbie, Modified discrete ordinates solution of radiative transfer in two-dimensional rectangular enclosures, J. Quant. Spectrosc. Radiat. Transf. 57 (1) (1997) 107–140, doi:10.1016/S0022-4073(96)00090-8.

[22] R.A. Ramankutty, A.L. Crosbie, Modified discrete-ordinates solution of radiative transfer in three-dimensional rectangular enclosures, JQSRT 60 (1) (1998) 103–134, doi:10.1016/S0022-4073(97)00026-5.

[23] H. Amiri, S.H. Mansouri, P.J. Coelho, Application of the modified discrete ordinates method with the concept of blocked-off region to irregular geometries, Int. J. Therm. Sci. 50 (4) (2011) 515–524, doi:10.1016/j.ijthermalsci.2010.10.012.

[24] R.-R. Zhou, B.-W. Li, The modified discrete ordinates method for radiative heat transfer in two-dimensional cylindrical medium, Int. J. Heat Mass Transf. 139 (2019) 1018–1030, doi:10.1016/j.ijheatmasstransfer.2019.05.071.

[25] J.R. Howell, M.P. Mengüç, K. Daun, R. Siegel, Thermal Radiation Heat Transfer, seventh ed., CRC press, 2020.

[26] P. Boulet, J. Gerardin, Z. Acem, G. Parent, A. Collin, Y. Pizzo, B. Porterie, Optical and radiative properties of clear PMMA samples exposed to a radiant heat flux, Int. J. Therm. Sci. 82 (2014) 1–8, doi:10.1016/j.ijthermalsci.2014.03.013.

[27] M.F. Modest, Radiative Heat Transfer, third ed., Academic press, 2013.

[28] A. Wang, M.F. Modest, High-accuracy, compact database of narrow-band k-distributions for water vapor and carbon dioxide, J. Quant. Spectrosc. Radiat. Transf. 93 (1-3) (2005) 245–261, doi:10.1016/j.jqsrt.2004.08.024.

[29] Y. Liu, J. Zhu, G. Liu, J.-l. Consalvi, F. Liu, A nongray-wall emissivity model for the wide-band correlated k-distribution method, Int. J. Heat Mass Transf. 159 (2020) 120095.

[30] A. Vali, D.S. Nobes, L.W. Kostiuk, Transport phenomena within the liquid phase of a laboratory-scale circular methanol pool fire, Combust. Flame 161 (4) (2014) 1076–1084, doi:10.1016/j.combustflame.2013.09.028.

[31] A. Vali, D.S. Nobes, L.W. Kostiuk, Fluid motion and energy transfer within burning liquid fuel pools of various thicknesses, Combust. Flame 162 (4) (2015) 1477–1488, doi:10.1016/j.combustflame.2014.11.013.

[32] P.A. Beaulieu, N.A. Dembsey, Flammability characteristics at applied heat flux levels up to 200 kw/m2, Fire Mater. 32 (2) (2008) 61–86, doi:10.1002/fam.948.

[33] M.F. Modest, Narrow-band and full-spectrum k-distributions for radiative heat transfer-correlated-k vs. scaling approximation, J. Quant. Spectrosc. Radiat.Transf. 76 (1) (2003) 69–83, doi:10.1016/S0022-4073(02)00046-8.